Since January 2020 Elsevier has created a COVID-19 resource centre with free information in English and Mandarin on the novel coronavirus COVID-19. The COVID-19 resource centre is hosted on Elsevier Connect, the company's public news and information website.

Life Sciences 324 (2023) 121750

Contents lists available at ScienceDirect

Life Sciences

journal homepage: www.elsevier.com/locate/lifescie

Acute coronavirus infection triggers a TNF-dependent osteoporotic phenotype in mice

Celso M. Queiroz-Junior [a,*], Anna C.P.M. Santos [b], Matheus R. Gonçalves [b], Camila B. Brito [b], Breno Barrioni [d], Pedro J. Almeida [e], Marcela H. Gonçalves-Pereira [c], Tarcília Silva [f], Sicília R. Oliveira [f], Marivalda M. Pereira [g], Helton C. Santiago [c], Mauro M. Teixeira [c], Vivian V. Costa [a,c,*]

[a] Department of Morphology, Institute of Biological Sciences, Universidade Federal de Minas Gerais, Belo Horizonte, MG, Brazil
[b] Department of Microbiology, Institute of Biological Sciences, Universidade Federal de Minas Gerais, Belo Horizonte, MG, Brazil
[c] Department of Biochemistry and Immunology, Institute of Biological Sciences, Universidade Federal de Minas Gerais, Belo Horizonte, MG, Brazil
[d] Institute of Engineering, Science and Technology, Universidade Federal dos Vales do Jequitinhonha e Mucuri, Janaúba, MG, Brazil
[e] Medical School, Ciências da Saúde: Infectologia e Medicina Tropical, Universidade Federal de Minas Gerais, Belo Horizonte, MG, Brazil
[f] Department of Oral Surgery and Pathology, School of Dentistry, Universidade Federal de Minas Gerais, Belo Horizonte, MG, Brazil
[g] Department of Metallurgical Engineering and Materials, School of Engineering, Universidade Federal de Minas Gerais, Belo Horizonte, MG, Brazil

ARTICLE INFO

Keywords:
Covid-19
Bone resorption
Coronavirus
MHV
Femur

ABSTRACT

Aims: Millions of people died during the COVID-19 pandemic, but the vast majority of infected individuals survived. Now, some consequences of the disease, known as long COVID, are been revealed. Although the respiratory system is the target of Sars-CoV-2, COVID-19 can influence other parts of the body, including bone. The aim of this work was to investigate the impact of acute coronavirus infection in bone metabolism.
Main methods: We evaluated RANKL/OPG levels in serum samples of patients with and without acute COVID-19. *In vitro*, the effects of coronavirus in osteoclasts and osteoblasts were investigated. *In vivo,* we evaluated the bone phenotype in a BSL2 mouse model of SARS-like disease induced by murine coronavirus (MHV-3).
Key findings: Patients with acute COVID-19 presented decreased OPG and increased RANKL/OPG ratio in the serum *versus* healthy individuals. *In vitro*, MHV-3 infected macrophages and osteoclasts, increasing their differentiation and TNF release. Oppositely, osteoblasts were not infected. *In vivo*, MHV-3 lung infection triggered bone resorption in the femur of mice, increasing the number of osteoclasts at 3dpi and decreasing at 5dpi. Indeed, apoptotic-caspase-3^{+} cells have been detected in the femur after infection as well as viral RNA. RANKL/OPG ratio and TNF levels also increased in the femur after infection. Accordingly, the bone phenotype of TNFRp$55^{-/-}$ mice infected with MHV-3 showed no signs of bone resorption or increase in the number of osteoclasts.
Significance: Coronavirus induces an osteoporotic phenotype in mice dependent on TNF and on macrophage/osteoclast infection.

1. Introduction

In March 2020, the World Health Organization (WHO) declared the acute respiratory coronavirus disease 2019 (COVID-19) a pandemic. Over 755 million cases of Sars-CoV-2 infection and over 6.8 million deaths have been reported globally as of 15 February 2023 [1]. Since then, much has been learned to develop vaccines and therapy protocols [2], but much still has to be studied. The infection first manifests in the respiratory tract, with variable symptoms, from dry cough and fever to acute respiratory distress syndrome and respiratory failure in severe cases [3]. Nevertheless, relevant extrapulmonary complications accompany these primary pulmonary signs [4].

Several COVID-19 patients experience anosmia, ageusia, diarrhea, headache, fatigue, cognitive dysfunction and other symptoms that go far beyond the lung disease [5,6]. Indeed, some evidence suggests that COVID-19 can even impact the musculoskeletal system [7,8]. Muscle,

* Corresponding authors at: Departamento de Morfologia, Instituto de Ciências Biológicas, Universidade Federal de Minas Gerais, Avenida Antônio Carlos, 6 627, Pampulha, CEP 31 270-901 Belo Horizonte, MG, Brasil.
E-mail addresses: cmqj@ufmg.br (C.M. Queiroz-Junior), vivianvcosta@ufmg.br (V.V. Costa).

https://doi.org/10.1016/j.lfs.2023.121750
Received 22 February 2023; Received in revised form 24 April 2023; Accepted 27 April 2023
Available online 2 May 2023

joint pain and bone burning have been reported in acute and chronic phases of COVID-19 [9,10]. There is evidence of reduced bone mineral density in patients subjected to intensive care and association with worse prognosis [11,12]. Experimentally, Sars-CoV-2 induced bone resorption in transgenic mice expressing human ACE-2 (Angiotensin Converting Enzyme 2), the enzyme required for viral entry in human cells [13]. Qiao et al. [14] demonstrated the inflammatory milieu triggered by Sars-CoV-2 as a pathway to explain the osteoporotic phenotype of infected hamsters. Nevertheless, lack more evidence to better understand the coronavirus-induced bone loss.

In a life-threatening condition such as COVID-19, to study musculoskeletal consequences of the disease can be seen as secondary, despite the impact bone disorders cause on health, economic and social contexts [15,16]. Moreover, there are limitations of infrastructure imposed to experimentally work with Sars-CoV-2: a biosafety level 3 (BSL3) laboratory is required; animals susceptible to the infection are needed, such as transgenic mice or hamsters; experimental tools to work with hamsters are not promptly available [17]. Thus, to overcome these limitations and allow the spread of new knowledge, our research group described a BSL2 mouse model that recapitulates several aspects of the acute phase of severe COVID-19 in wild type mice, using a murine betacoronvirus, MHV-3 [18]. The MHV (mouse hepatitis virus) belongs to the coronavirus family of enveloped positive-strand RNA viruses and it is a natural pathogen of mice [19]. Upon intranasal inoculation, MHV-3 triggers a transient lung inflammation after 3 days, with viral replication, lung damage, respiratory dysfunction, and systemic commitment of mice [18].

Therefore, the aim of this work was to investigate the impact of acute coronavirus infection on bone metabolism. First, we investigated the serum levels of RANKL and osteoprotegerin in patients with acute COVID-19. We also evaluated the effect of MHV-3 infection in osteoclasts and osteoblasts *in vitro* and the acute bone loss induced by coronavirus *in vivo*. Finally, we investigated the role of TNF in the bone phenotype associated with the SARS-like disease induced by MHV-3 in mice.

2. Methods

2.1. Human serum samples

Forty-five patients with acute COVID-19 were recruited as part of the exploratory outcomes of the RESOLVIR trial, approved by the National Research Ethics Commission (Comissão Nacional de Ética em Pesquisa - 35449720.7.0000.5149). The patients were admitted to Eduardo de Menezes Hospital (Belo Horizonte, Brazil), the reference center for infectious diseases in the state of Minas Gerais, with COVID-19 infection confirmed by Reverse Transcriptase-Polimerase Chain Reaction (RT-PCR) tests in 2021. All patients had severe acute respiratory syndrome (SARS) and required oxygen support. Only samples acquired at baseline of the phase two patients were used in these analyses. As per city protocol at the time, patients were in use of Dexamethasone 10 mg/day, ceftriaxone and azithromycin. Forty-five serum samples obtained from healthy individuals matched for gender and age were used as controls. These Control samples were obtained before the pandemic, in 2018 (Comissão Nacional de Ética em Pesquisa - 24832513.4.0000.5149), in the region of the Centro de Saúde Jardim Montanhês (Belo Horizonte, Brazil). All patients agreed to participate in the study and provided signed informed consent. In Covid-19 and Control groups, serum samples were obtained and serum markers of bone metabolism, RANKL and OPG, were analyzed by ELISA.

2.2. RAW264.7 cell culture and osteoclast differentiation

Immortalized RAW264.7 cells were used to characterize the effects of MHV-3 infection in macrophages and osteoclast differentiation. The cells were cultured in DMEM medium (Cultilab) supplemented with 10 % fetal bovine serum (FBS; Gibco), in culture flasks. After achieving optimal confluence, cells were plated at a concentration of 1×10^3 cells/well for 96-well plates or 1×10^4 cells/well for 24-well plates. For osteoclast differentiation, cells were stimulated with 50 ng/ml of receptor activator of nuclear factor-kB ligand (RANKL, Peprotech) every two days for one week. After differentiation, cells were stimulated with MHV-3 at MOI 0.1 / 0.01 / 0.001. After 12, 24 or 48 h of virus challenge the cultures of macrophages and osteoclasts were evaluated for cell viability by MTT, TRAP assay and virus titration in the supernatant. Quantification of cytokines in the supernatant was also evaluated by ELISA using the MOI 0.001 at 12 h after infection.

2.3. Culture of immortalized osteoblasts

In the experiments with osteoblasts, MC3T3-E1 cell line, subclone 14 (immortalized pre-osteoblasts from the skull of neonate mice (American Type Culture Collection, Arlington, VA)) was used. Cells were grown in osteogenic medium [minimal essential medium (αMEM, Gibco) with 10 % FBS (Gibco); 100 μg/ml gentamicin; 5 μg/ml ascorbic acid (Sigma-Aldrich, USA); and 2.16 mg/ml β-glycerophosphate (Sigma-Aldrich)]. The medium was changed every 2 d for one week. Afterwards, the cells were counted and plated at a concentration of 5×10^3 for 24-well plates and 5×10^2 for 96-well plates. Twenty-four hours after plating, cells were stimulated with MHV-3 at MOI 0.1 / 0.01 / 0.001. Cell viability assay by MTT and virus titration in the supernatant were performed 12, 24 or 48 h after viral challenge. The alkaline phosphatase and alizarin red assay were performed 7 and 14 d after infection, with MOI 0.01.

2.3.1. Alkaline phosphatase assay

Alkaline phosphatase enzyme activity was evaluated in osteoblasts using the NBT / BCIP (nitro-blue tetrazolium/5-bromo-4-chloro-3 indolyl phosphate) assay, after stimulation with MHV-3. The wells were washed with PBS and the NBT/BCIP solution [1 (NBT): 1 (BCIP): 8 (PBS)] (Invitrogen) has been added. After incubation (37 °C for 2 h), a solution of 10 % SDS and 0.3 % HCl in water was added and the plates were incubated (37 °C overnight). The following day, the optical density of the supernatant was read in a spectrophotometer at 595 nm.

2.3.2. Alizarin red assay

The evaluation of mineralized matrix production by osteoblasts was performed with the alizarin red method after infection with MHV-3. The Mc3t3 cells were grown on glass coverslips, in 24-well culture plates. At the end of the experiment, the wells were washed with PBS, fixed with 4 % glutaraldehyde in PBS for 15 min. Then, the alizarin red solution (40 mM, pH 4.2) was added and shaked for 20 min. The dye was removed, the wells were washed with distilled water and the coverslips were mounted on slides, which were photographed for analysis. 5 fields were photographed on each coverslip (4× magnification; totalizing ~17 mm^2) and the area with mineralized matrix was quantified using ImageJ software.

2.4. Virus titration

To measure viable viral titers in cell culture, we performed the titration protocol in immortalized L929 cells, which are permissive to MHV-3 (ATCC CCL-1). Cells were expanded with DMEM medium supplemented with 10 % FBS and plated in 24-well plates at a concentration of 1×10^5 cells per well. Twenty-four hours after plating, the supernatants from the osteoclast and osteoblast experiments were serially diluted with DMEM, pipetted over the cells and incubated for 1 h under agitation. Afterward, overlay medium (DMEM containing 1.6 % carboxymethylcellulose) was added and kept for 2 days at 37 °C and 5 % CO_2. Then, cells were fixed with 10 % neutral buffered formalin (NBF) for 1 h and stained with 0.1 % crystal violet. Virus titers were determined as PFU/ml.

2.5. MTT cell viability assay

The MTT assay was performed to measure the viability of Raw 264.7 macrophages, osteoclasts and osteoblast. After stimulation with MHV-3, the wells were washed with PBS and a solution of MTT (1 mg/ml) in α-MEM or D-MEM was added. After incubation (4 h at 37 °C and 5 % CO_2), another wash was performed and the isopropanol/HCl solution was added to dilute the formazan crystals. The supernatant was quantified by measuring the absorbance values at 595 nm, in a spectrophotometer.

2.6. Mice

Male and female wild-type C57BL/6 mice (Central Animal House UFMG) and TNF receptor knockout mice (TNFRp55$^{-/-}$, stock no.002818; Jackson Laboratories), aged between 6 and 8 weeks, were used throughout the experiments. Mice were housed in individual ventilated cages in an animal care facility with 12/12 h light/dark cycle at 23–25 °C and free access to food and water. The *in vivo* experimental procedures were approved by the UFMG Ethics Committee for the Use of Animals (process no. 190/2020).

2.7. MHV-3 infection

Mice were divided into a Mock control group and two groups infected with MHV-3 (one with 3 and the other with 5 days of infection). They were anesthetized intraperitoneally [ketamine (50 mg/kg) xylazine (5 mg/kg)] and received an intranasal inoculum of 30 μl of sterile saline with MHV-3 (10^3 PFU). Mock animals received only the vehicle. On the last day of the experiment, the animals were euthanized and the lung and femur were collected for analysis.

2.8. Histological analysis

Tissues extracted for histological analysis were fixed in 10 % formalin at pH 7.4 for 48 h. The femur samples underwent a decalcification process in 14 % EDTA for 1 month. Tissues were dehydrated in graded ethanol, and embedded in paraffin. Serial sections (5 μm) were stained with hematoxylin and eosin (H&E), Masson's trichrome, TRAP or immunohistochemistry. The lung slides were stained with H&E and were examined for determination of the inflammation-mediated injury using a score system encompassing (i) airway inflammation (up to 4 points), (ii) vascular inflammation (up to 4 points), (iii) parenchyma inflammation (up to 5 points), and neutrophil infiltration (up to 5 points). Bone slides stained with H&E were photographed in the distal region of the femur, next to the epiphyseal cartilage, and were evaluated for the percentage of trabeculae in relation to the total evaluated area, using the ImageJ software (National Institutes of Health, Bethesda, USA). Femur slides were also stained with Masson's trichrome for osteoblast cell counts. Osteoblasts were identified by their position next to bone trabeculae and their morphological characteristics. The cells were counted and data were expressed as number of cells per microscopic field (magnification: 400×).

2.9. TRAP assay

The TRAP assay was performed in bone samples and in macrophage/osteoclast cell cultures. For the femur samples extracted from animal experiments, the tissues were decalcified, processed, embedded and sectioned into 5-mm thickness slices. For the *in vitro* experiments the TRAP assay was performed, after stimulation with MHV-3, in cells cultured on coverslips. In both cases, staining was performed with the acid phosphatase leukocyte (TRAP) Kit (Sigma-Aldrich), following the manufacturer's instructions. Osteoclasts were identified as TRAP-positive cells adjacent to bone trabeculae. For the *in vitro* data, the cells were photographed (20× magnification) for counting the TRAP-positive cells and the multinucleated (two or more nuclei) TRAP-positive cells. The area of each multinucleated TRAP-positive cell was also measured using Image-J.

2.10. Immunohistochemistry

Bone slides were also processed for immunohistochemistry (IHC). IHC slides were deparaffinized, hydrated and endogenous peroxidase blockade was performed with 0.3 % hydrogen peroxide. Antigen retrieval was performed with 0.1 M citrate buffer solution. The sections were then coated with primary rabbit anti-mouse cleaved Caspase-3 antibody (1:300; Cell Signaling Technology (Asp175 - #9961)), for labeling cleaved Caspase-3. Then the sections were incubated with the secondary antibody (VECTASTAIN Elite ABC HRP Kit) and stained with DAB chromogenic solution (Sigma-Aldrich). Counterstaining with hematoxylin was performed. Negative reaction controls comprised samples in which the primary antibodies were omitted.

2.11. MicroCT analysis

The samples of femur were scanned using a compact desktop micro-CT scanner (SkyScan 1174, Bruker micro-CT, Belgium), with 50 kV of source voltage, 800 μA source current and 8.05 μm pixel size. A 0.5 mm aluminium filter was used. The samples were attached to a stage that rotated 180° with images acquired every 0.7°. The acquired shadow projections (16-bit TIFF format) were further reconstructed into 2D slices using the NRecon software interface (Skyscan, Bruker micro-CT, Belgium). CTAn software (Skyscan, Bruker Micro-CT, Belgium) was used for 3D analyses, and CTVox (Skyscan, Bruker Micro-CT, Belgium) was applied for the 3D bone volume observation. The parameters evaluated were trabecular separation (Tb.Sp), percent bone volume (BV/TV), trabecular thickness (Tb.Th) and porosity percentage.

2.12. RT-PCR for MHV-3 detection

Viral RNA was extracted with the QIAamp® Viral RNA kit, following the manufacturer's instructions. The femur samples were macerated with the lysis buffer, eluted and the RNA was quantified in a spectrophotometer (NanoDrop™ , Thermo Scientific). cDNA was synthetized with 500 ng of total RNA using the iScript™ gDNA Clear cDNA Synthesis Kit (BIO-RAD) following the manufacturer's instructions. The cDNA was then diluted 1:10 to be used in the qPCR assay with Fast SYBR™ Green Master Mix (Applied Biosystems™) and primers in concentration of 5 nM: Forward primer 5′-CAGATCCTTGATGATGGCGTAGT-3′; Reverse primer 5′-AGAGTGTCCTATCCCGACTTTCTC-3′. The standard was obtained by extracting RNA from a known amount of PFU from MHV-3. Results were expressed in Relative Units/500 ng cDNA.

2.13. ELISA

Cytokines associated with bone remodeling were quantified by ELISA in *in vivo* and *in vitro* experiments and in the serum samples of patients. In samples from patients with or without COVID-19, serum RANKL and OPG levels were quantified. For determination of the RANKL/OPG ratio of each patient, samples which presented undetected levels of RANKL or OPG were excluded. In the animal femur samples, RANKL, OPG, TNF and IL-1β were evaluated. We also performed ELISA for supernatant samples of macrophages/osteoclasts (TNF) or Mc3t3 (IL-6) cells. All assays were performed using standard ELISA kits (R&D Systems), according to the manufacturer's recommendations. The results are expressed as picograms of cytokine per ml/100 mg tissue.

2.14. Statistical analysis

Quantitative data were expressed as mean ± standard error of the

mean. Differences between means were assessed by unpaired Student's *t*-test or one-way ANOVA followed by Tukey's multiple comparisons test when data presented normal distribution. Data presenting non-normal distribution were evaluated using the non-parametric Mann-Whitney test. Differences with $p < 0.05$ were considered statistically significant.

3. Results

3.1. Acute COVID-19 decreases serum levels of OPG and increases RANKL/OPG ratio in patients

The first step of this study was to investigate whether COVID-19 impacts serum levels of RANKL and OPG, mediators that induce and prevent osteoclastogenesis respectively, in patients with acute disease. To that end, a total of 45 patients with COVID-19 requiring hospital admission for oxygen therapy were recruited in 2021. COVID-19 diagnostic was confirmed by PCR test. There were 22 women (mean age (SD): 52.27 (8.84) years old; min. 32, max. 65) and 23 men (mean age (SD): 50.56 (12.49) years old; min. 27, max. 70). In their first appointment for hospital admission, serum samples were collected for evaluation of RANKL and OPG levels. Serum samples from healthy gender and age-matched individuals, collected before the pandemic, were used as controls (22 women: mean age (SD): 52.27 (8.84), min. 32, max. 65; and 23 men: mean age (SD): 48.96 (12.27), min. 27, max. 70). The mean serum levels of RANKL (132.5 (±147.8) pg/ml in controls *versus* 281.7 (±937.4) pg/ml in COVID-19 patients) reached no statistical difference between the groups (Fig. 1A). In contrast, OPG serum levels were significantly decreased in the samples of patients with COVID-19 when compared to matched controls (Fig. 1B). No correlation was detected between RANKL/OPG serum levels and age or gender of the patients. Nevertheless, the decrease in OPG concentration translated into high serum RANKL/OPG ratio during COVID-19 (Fig. 1C), which may impact bone metabolism in acute and long term.

3.2. Coronavirus infects osteoclasts but does not affect osteoblasts

Raw 264.7 macrophages, stimulated or not with RANKL for osteoclast differentiation, were susceptible to productive MHV-3 infection. The murine coronavirus propagated in these cells and progressively decreased cell viability just after 48 h (Fig. 2A-D). Both in the absence or presence of RANKL, MHV-3 triggered macrophage fusion, with syncytial formations which were positive for TRAP (Fig. 2E-F,H), the characteristic enzyme of osteoclasts. The multinucleated cells had significantly higher size in the presence of MHV-3, when compared to non-infected osteoclasts (Fig. 2G). Such phenotype associated to increased TNF release by RANKL-stimulated osteoclasts just after 12 h of infection (Fig. 2J).

In contrast, osteoblasts derived from MC3t3 cells were not susceptible to MHV-3 infection. No viral titer was detected in this cell culture (data not shown) and no effect was observed on cell viability (Fig. 2K). MHV-3 did not influence osteoblast activity and mineralization pattern, as indicated by IL-6 release (Fig. 2L), alkaline phosphatase (Fig. 2M) and alizarin red staining of mineral nodules (Fig. 2N-O). Thus, MHV-3 coronavirus triggered osteoclast differentiation but did not affect osteoblast.

3.3. Lung infection with the betacoronavirus MHV-3 triggers bone resorption in mice

In view of the current human data and *in vitro* evidence of the potential influence of coronavirus infection on bone metabolism, we investigated the effects of MHV-3 infection in the bone of mice. In accordance with previous published data of our group [18], MHV-3 intranasal infection triggered significant lung damage at 3 days post virus inoculation (Fig. 3A). There was transient recruitment of leukocytes, including mononuclear and polymorphonuclear cells, especially to perivascular areas of the lung parenchyma, and hyperplasia of the alveolar walls, which decreased after 5 dpi (Fig. 3A-B). This experimental model is characterized by significant viral titers in the lung (10^4 PFU/g) but mild systemic commitment at 3 dpi, with viremia been detected only at 5 dpi [18]. In this way, we investigated whether bone phenotype could be influenced in the acute phase of lung disease.

Indeed, MHV-3 infection induced a significant decrease in trabecular number at 3 dpi at the distal region of the femur of infected mice (Fig. 3C-D). Microcomputed tomography showed that MHV-3 infected mice had reduced trabecular bone volume fraction (Fig. 3E, I) and trabecular thickness (Fig. 3F, I) at 3 dpi, although porosity and trabecular separation (Fig. 3G-I) only increased significantly at 5 dpi, indicating that the process started acutely with the lung disease and progressed with the systemic commitment.

3.4. MHV-3 infection increases the number of osteoclasts and RANKL/OPG ratio in the femur of mice

The trabecular bone resorption observed in the femur of infected mice associated with increased number of TRAP-positive osteoclasts lining the trabeculae surface at 3 days post-MHV-3 infection (Fig. 4A-B). Interestingly, these TRAP-positive cells have not been detected significantly at 5 dpi (Fig. 4A-B), which may indicate cell death. Indeed, there were signs of apoptosis with the detection of apoptotic bodies and cleaved caspase-3-positive cells adjacent to the trabecular surfaces (Fig. 4C-D) after MHV-3 infection. As shown in the *in vitro* results, osteoclasts can be infected and die after infection, and viral RNA copies have been detected in the femur of mice just after 3 dpi (Fig. 4E). Regarding osteoblasts, infection of mice with the betacoronavirus MHV-3 did not induce any effect on the number of these cells (Fig. 4F-G), which indicates that the viral induced-bone resorption is primarily associated with osteoclast stimulation.

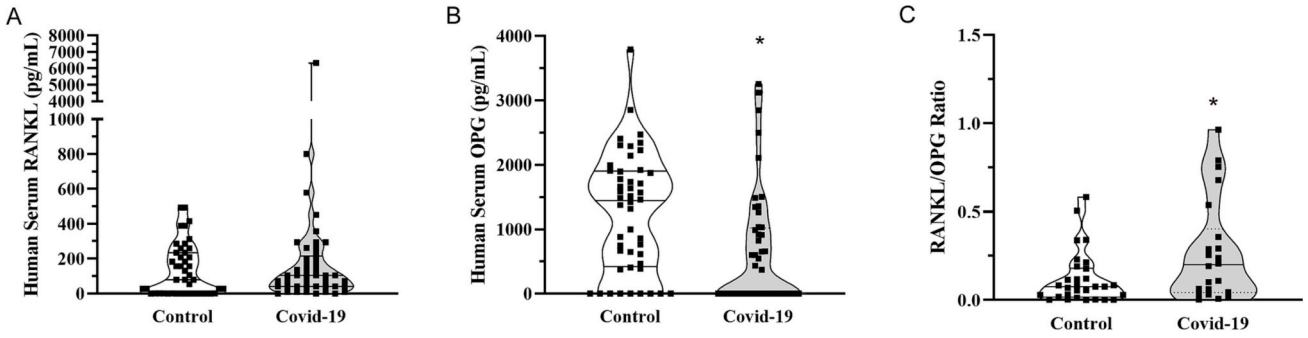

Fig. 1. Serum levels of RANKL and OPG in patients with acute COVID-19. Serum samples were collected from patients with and without COVID-19 ($n = 45$ matched patients per group) and evaluated for (A) RANKL and (B) osteoprotegerin (OPG) by ELISA. (C) RANKL/OPG ratio was evaluated excluding the undetected values of RANKL or OPG. * $p < 0.05$, Mann-Whitney test.

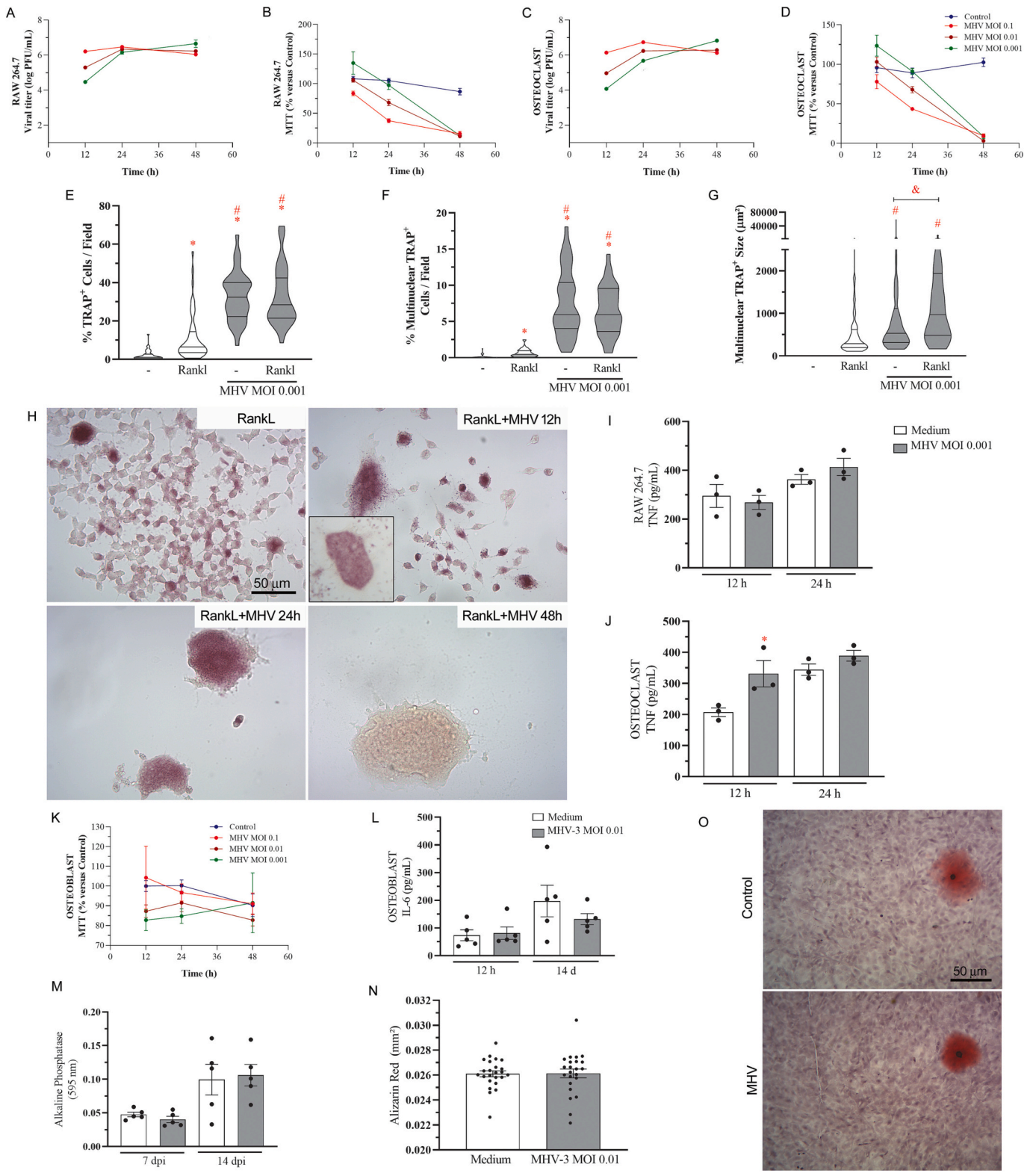

Fig. 2. MHV-3 infects macrophages and osteoclasts, but not osteoblasts. Viral titers and cell viability (MTT assay) were detected in (A-B) Raw 264.7 macrophages and in (C—D) Rankl-stimulated osteoclasts12, 24 and 48 h after infection with MHV-3 at MOI 0.1, 0.01 and 0.001. (E) Quantification of total TRAP-positive cells, (F) multinucleated TRAP-positive cells, and (G) area of individual multinucleated cells 12 h after MHV-3 infection at MOI 0.001. (H) Representative photomicrographs from osteoclast cell culture. (I-J) TNF was quantified in macrophage and osteoclast cell culture supernatants 12 and 24 h after MHV-3 stimulation. (K) Osteoblast viability (MTT assay) 12, 24 and 48 h after MHV-3 stimulation. (L) IL-6 was quantified by ELISA in osteoblast cell culture supernatant 12 h and 14d after MHV-3 stimulation. (M) Alkaline phosphatase activity was detected colorimetrically 14 d after cell stimulation. (G) Alizarin red was quantified morphometrically 14 d after MHV-3 stimulation. (H) Representative images of alizarin red stained osteoblast samples. * $p < 0.05$ *versus* Control group. # $p < 0.05$ *versus* RankL group. Statistical evaluation was performed using Student's *t*-test for comparison of two independent groups and one-way ANOVA followed by the Tukey's multiple comparisons test for more than two groups.

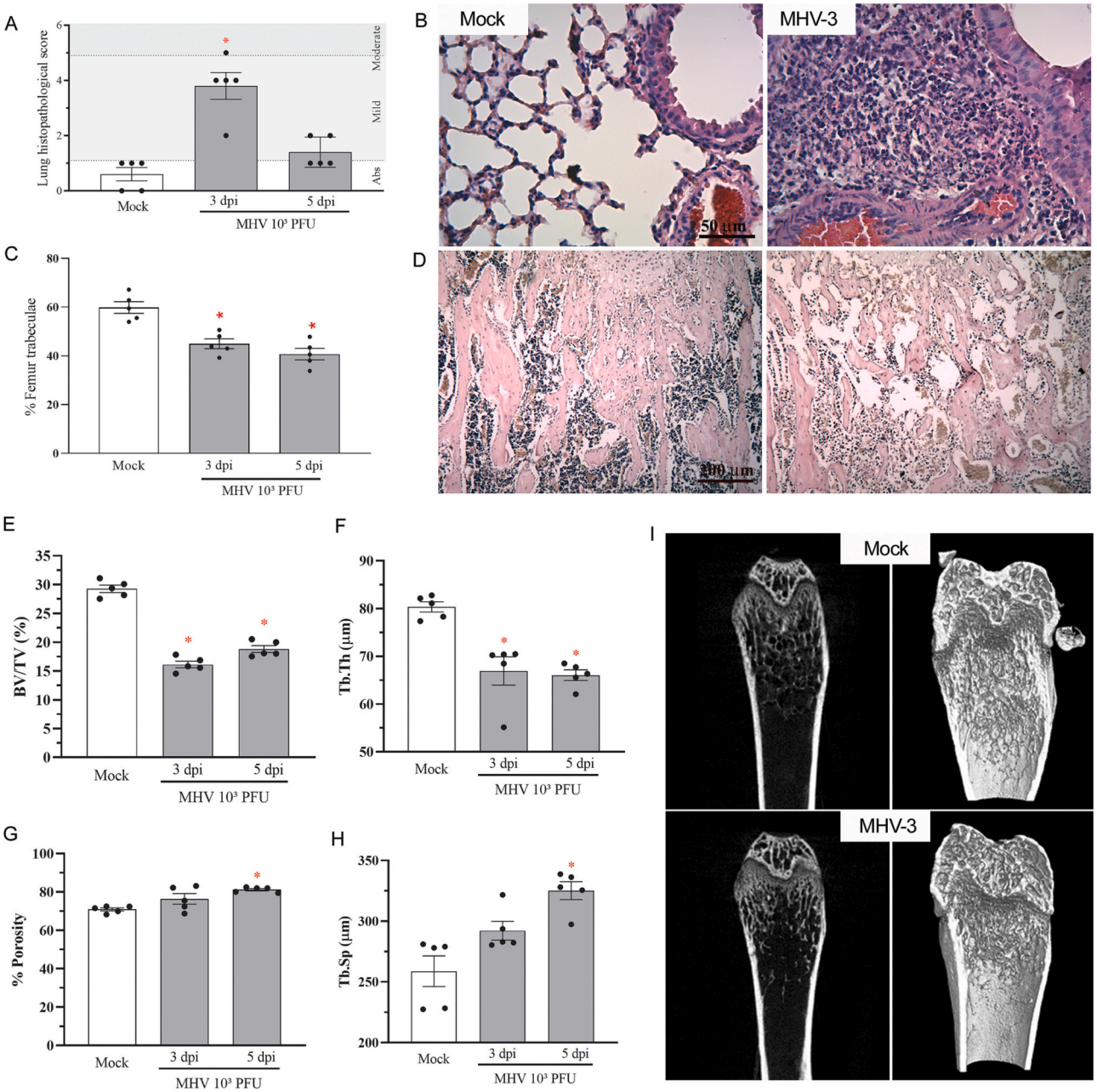

Fig. 3. MHV-3 lung infection triggers trabecular bone resorption. (A) Mice lung inflammatory score upon MHV-3 infection. (B) H&*E*-stained lung sections showing significant signs of inflammatory injury in infected mice, including inflammatory cell infiltrate and pyknosis, which indicate cell death. Scale bar, 50 µm. (C) Morphometric quantitation of percentage of trabecular bone in the distal region of the femur. (D) Representative H&E-stained bone sections showing decreased trabecular bone in the MHV-3 infected group, when compared to the Mock group. Scale bar, 200 µm. MicroCT analysis of (E) percent bone volume (BV/TV), (F) trabecular thickness (Tb.Th), (G) porosity percentage and (H) trabecular separation (Tb.Sp). (I) Representative 2D and 3D microCT images of Mock and MHV-3-infected femur samples. * $p < 0.05$ *versus* Mock group. Statistical evaluation was performed using one-way ANOVA followed by the Tukey's multiple comparisons test.

In accordance with the phenotype of bone resorption induced by MHV-3 infection, we investigated the expression of bone-related mediators. The lung viral infection triggered an increase in bone RANKL expression and the RANKL/OPG ratio at 5 dpi, but not at 3 dpi (Fig. 4H-J). Similarly, the expression of TNF, a cytokine directly related to bone resorption, showed an increasing pattern in the femur of infected mice, that reached statistical significance at 5 dpi (Fig. 4K). No difference was detected in the levels of IL-1β in the femur of infected mice (Fig. 4L).

3.5. MHV-3-induced bone loss is dependent on TNF

As a proof of concept, we investigated whether MHV-3 intranasal infection would trigger bone resorption in TNFR$^{-/-}$ mice. As shown by our group previously, the absence of TNF receptor improved the course of the disease induced by MHV-3, with significantly reduced lung damage and systemic commitment in TNFR$^{-/-}$ mice [18]. Accordingly, the infection of TNFR$^{-/-}$ mice with the betacoronavirus MHV-3 did not induce trabeculae resorption as occurred in WT mice at 3 dpi (Fig. 5A-B). Microcomputed tomography showed that the femur of infected TNFR$^{-/-}$ mice had similar trabecular bone fraction, trabecular thickness,

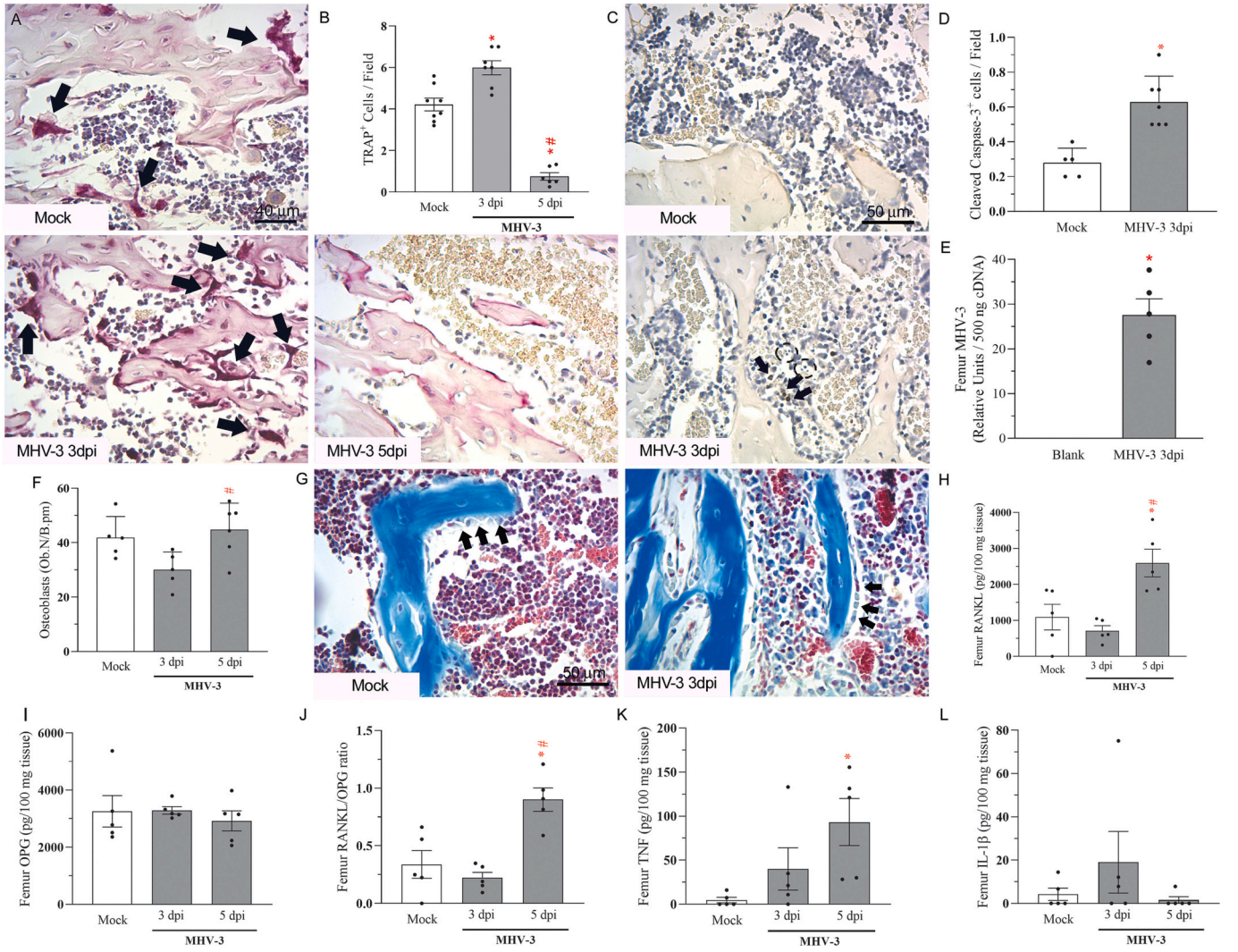

Fig. 4. MHV-3 lung infection increases osteoclast number and RANKL levels in the femur. (A) Representative TRAP-stained femur slides of Mock, MHV-3 3dpi and MHV-3 5dpi mice. Arrows: TRAP-positive osteoclasts. Scale bar, 40 μm. (B) Quantitation of TRAP-positive cells next to bone trabeculae in 400×-magnification fields. (C) Representative images of cleaved caspase-3 stained slides of Mock and MHV-3-infected samples at 3dpi. Arrows: Cleaved Caspase-3 positive cells; Dotted circles: apoptotic bodies. Scale bar, 50 μm. (D) Quantitation of cleaved caspase-3 positive cells per 400× magnification field in the femur of mice. (E) MHV-3 detection in the femur of infected mice at 3dpi by qPCR. (F) Quantitation of osteoblasts lining trabecular surfaces in Mock and MHV-3 infected samples. (G) Representative Masson's Trichrome stained femur samples showing osteoblasts next to trabeculae. Arrows: morphologically active osteoblasts. Femur levels of (H) RANKL, (I) osteoprotegerin (OPG), (J) RANKL/OPG ratio, (K) TNF and (L) IL-1β detected by ELISA. * $p < 0.05$ *versus* Mock group; # $p < 0.05$ *versus* MHV-3 3dpi group. Statistical analysis was performed using one-way ANOVA followed by the Tukey's multiple comparisons test.

porosity and separation as their non-infected littermates (Fig. 5C-G). In line with these results, while WT mice had increased TRAP-positive cells at 3 dpi, the number of osteoclasts was not affected by MHV-3 infection in TNFR$^{-/-}$ mice (Fig. 5H-I). These results indicate that bone resorption triggered by MHV-3 is dependent on TNF p55 receptor.

4. Discussion

The possible systemic commitment observed in acute and chronic COVID-19 stages is just been discovered as the pandemic progresses and slows. There is now strong evidence of several potential extra-pulmonary effects induced by Sars-CoV-2 infection, such as neurological-related conditions, including anosmia, ageusia, headache, and cognitive dysfunction [5,6], cardiovascular disorders, such as microangiopathy and thrombotic events [20], problems in male fertility [21] and other multi-organ conditions. Among these, the evidence of bone metabolism disorders associated with coronavirus infection is just starting to be described. Here, we have shown that: 1. Patients with acute COVID-19 present decreased serum levels of OPG; 2. The beta-coronavirus MHV-3 can infect and increase the differentiation of osteoclasts; 3. MHV3 infection triggers bone resorption in the femur of mice; 4. The MHV-3 induced bone resorption is dependent on TNF.

The hypothesis suggesting that COVID-19 could affect the musculoskeletal system popped into the scientific literature just after the clinical consequences and cytokine storm induced by the infection were described [7,22]. The hospitalization of patients susceptible to severe cases of COVID-19 may lead to periods of immobilization and this can cause the called “immobility syndrome” with a component of loss of bone mass [23]. Moreover, treatment protocols for viral infections based on corticoid therapies are known to decrease bone mineral density (BMD), such as evidenced in the SARS-CoV outbreak [24]. Accordingly, severe COVID-19 was associated with low total body BMD in people over 60 years old [25]. Another report showed that patients requiring intensive care had a significantly lower BMD and this could be a prognostic information on the necessity for ICU treatment in the course of COVID-19 pneumonia [11]. In line with this evidence, hypercalcemia,

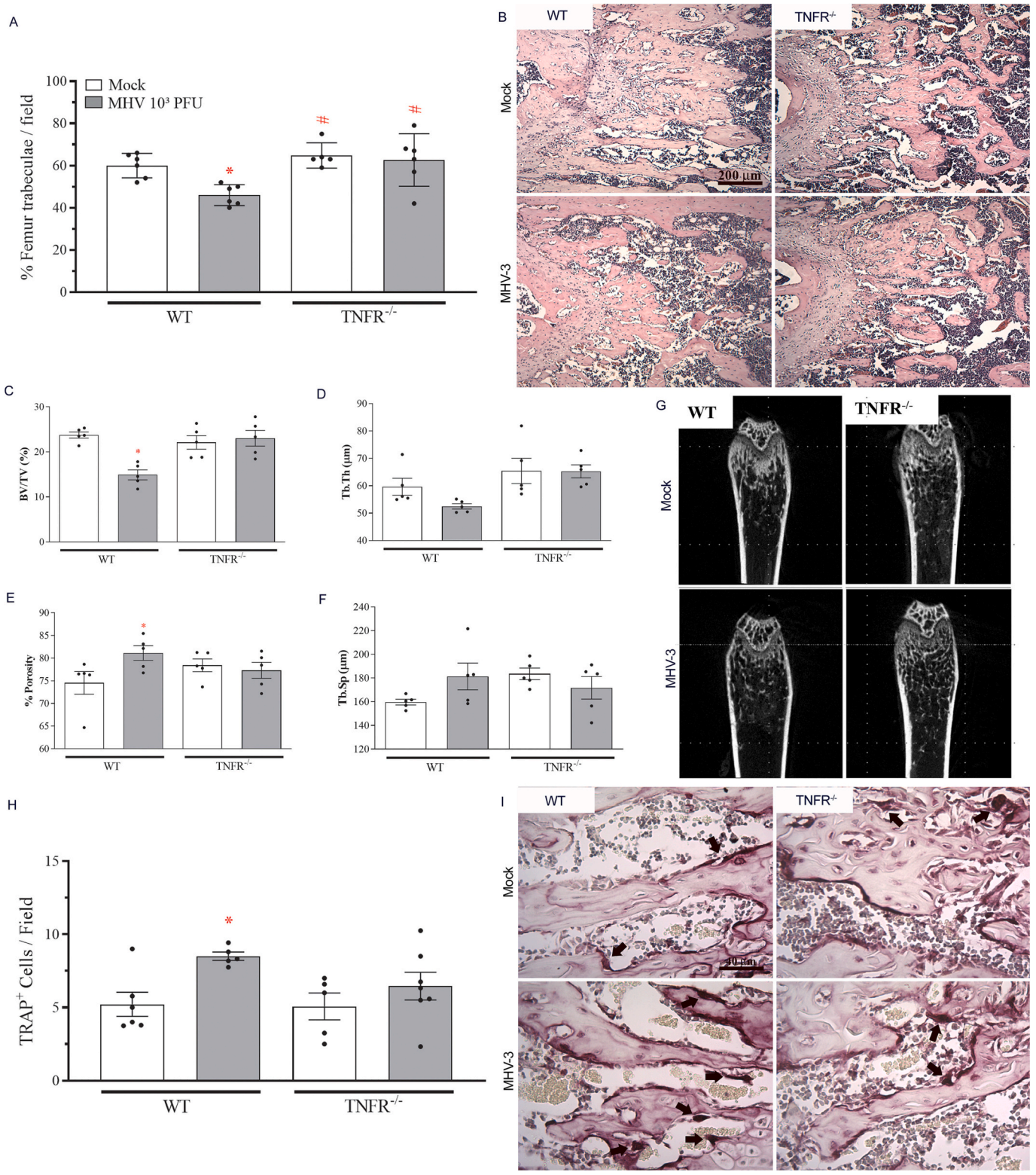

Fig. 5. MHV-3-induced bone loss is dependent on TNF. TNFR$^{-/-}$ mice were infected with MHV-3 and their euthanasia was conducted at 3dpi. (A) Morphometric quantitation of percentage of trabecular bone in the distal region of the femur. (B) Representative H&*E*-stained bone sections showing decreased trabecular bone in the MHV-3 WT infected group, when compared to the TNFR$^{-/-}$ infected group. Scale bar, 200 µm. MicroCT analysis of (C) percent bone volume (BV/TV), (D) trabecular thickness (Tb.Th), (E) porosity percentage and (F) trabecular separation (Tb.Sp). (G) Representative 2D microCT images of MHV-3-infected WT and TNFR$^{-/-}$ femur samples. (H) Quantitation of TRAP-positive cells next to bone trabeculae in 400×-magnification fields. (I) Representative TRAP-stained femur slides of Mock and MHV-3 WT and TNFR$^{-/-}$ femur samples. Arrows: TRAP-positive osteoclasts. Scale bar, 40 µm. * $p < 0.05$ *versus* the respective Mock group; # $p < 0.05$ *versus* WT infected group. Statistical analysis was performed using one-way ANOVA followed by the Tukey's multiple comparisons test.

which correlates to bone disease, also correlated to poorer survival rates in COVID-19 patients [26]. These clinical findings of bone resorption are in line with the current data of lower OPG serum levels and high RANKL/OPG ratio in patients with acute COVID-19. RANKL and OPG are the most significant mediators related to osteoclast differentiation and activation, being RANKL the stimulator and OPG the decoy-receptor of RANKL that inhibits osteoclast formation [27]. Thus, increased RANKL/OPG ratio, besides the cytokine storm, may translate to unbalance of osteoclast/osteoblast activity along coronavirus infection in favor of the bone resorptive milieu associated to osteoclasts.

In the current work, the experimental settings supported such clinical condition. The intranasal infection of WT mice with the betacoronavirus MHV-3 triggered significant decrease in trabecular area and bone volume in the distal region of the femur, as early as 3 days post infection. There was an osteoporotic phenotype associated to MHV-3 infection with increased number of TRAP-positive osteoclasts in the femur, although the number of osteoblasts was not affected. These data are in line with a recent study using human-ACE2 transgenic mice infected with Sars-CoV-2, which presented significant resorption of the trabecular bone in the femur in acute and post-recovery COVID-19. This phenotype was observed in mild and also in severe infection, developed with increasing viral titers [13]. A study with hamsters, which are naturally infected by Sars-CoV-2 and recover from the disease, also showed similar influence of Sars-CoV-2 on bone metabolism, in the femur and in the vertebrae [14]. Increased osteoclast differentiation was also detected in these works [13,14]. Interestingly, here the number of multinucleated osteoclasts increased at 3 dpi, but almost no TRAP-positive cells were detected in the femur at 5 dpi, even with high levels of local RANKL. This suggested osteoclast cell death.

Indeed, some authors hypothesize that bone cells could be themselves targets for coronavirus infection [8]. *In vivo*, we could detect MHV-3 RNA copies, caspase-3-positive cells and apoptotic bodies next to trabecular surface in the femur of infected mice. Accordingly, in our *in vitro* experiments, the betacoronavirus MHV-3 infected macrophages and differentiated osteoclasts, besides inducing increase in the number and size of TRAP-positive osteoclasts, even in the absence of RANKL. Almost all these cells died as early as 48 h after infection. MHV-3 is able to infect macrophages *via* the carcinoembryonic antigen-related cell adhesion molecule 1 (CEACAM-1a) receptor [19]. The presence of MHV-3 on bone marrow has also been described previously [28] as well as its ability to trigger syncytia formation [19]. Osteoclast differentiation is a coordinated process of macrophage fusion with the formation of multinucleated cells, as a syncytium [29], thus it is not surprising to notice TRAP-positive cells after MHV-3 macrophage infection in the absence of RANKL. Accordingly, there is potential evidence to support that this can also be true for Sars-CoV-2. Osteoclasts and osteoblasts can express the Angiotensin Converting Enzyme-2 (ACE2) which acts as a receptor for Sars-CoV-2 infection [30]. Human monocytes, which are precursors of macrophages, also express ACE2 [31] and are known to be infected by Sars-CoV-2 [32]. Similar to MHV-3, Sars-CoV-2 also triggers syncytial formation to facilitate viral dissemination, cytopathicity and immune evasion. The viral spike protein can interact with receptors on neighboring cells enhancing fusogenicity [33]. Thus Sars-CoV-2 could be a key player in osteoclast differentiation, but this remains to be shown.

Along with the potential direct effect of coronaviruses on bone cells, the cytokine storm triggered by the infection also creates a systemic inflammatory milieu conductive to bone resorption [4]. Severe COVID-19 is characterized by high circulating levels of TNF, IL-1β, IL-6 and several other cytokines that are known to be pro-osteoclastogenic, given that they favor the RANKL expression and release by osteoblasts and also immune cells [27,34]. In the current experimental settings, there was significant lung disease, but very mild systemic commitment, *i.e.* alterations in the liver, at 3 dpi. Nevertheless, viremia is detected at 5 dpi, with severe liver damage and systemic cytokine release which leads to fulminant mice death [18]. Accordingly, we have shown previously that the development of the lung disease triggered by MHV-3 infection was almost ablated in the absence of the TNF receptor type 1 [18]. Here, we show that this milder disease is relevant to prevent the potential bone disorder associated to the viral infection. $TNFR^{-/-}$ mice did not present significant signs of bone resorption and had decreased number of osteoclasts when compared to their WT littermates. This is in line with current evidence showing that TNF is a key mediator to trigger osteoclast formation in the context of COVID-19. TNF and IL-1β release induced by Sars-CoV-2 can amplify the pro-inflammatory cascade in the skeletal system to increase the pro-osteoclastogenic milieu [14]. Accordingly, some clinical trials targeting the TNF pathway have been started all over the world and there is evidence that an anti-TNF therapy abrogates the pathological inflammation and facilitates clinical recovery in severe COVID-19 [35,36]. As far as COVID-19 symptoms are prevented, the possibility of extra-pulmonary effects, such as bone resorption, may be prevented too.

Therefore, this study uses an experimental platform that recapitulates several aspects of COVID-19 to show the TNF-dependent bone resorptive phenotype triggered by the coronavirus infection, a condition that needs to be further investigated clinically. As any experimental model, there are limitations in the current settings, including: MHV-3 interacts with a receptor different from Sars-CoV-2, MHV-3 triggers liver disease in later timepoints, there is a transient lung disease. Nevertheless, this platform allows us to work in a BSL2 lab using WT mice and it triggers an acute lung disease that induces systemic commitment such as bone resorption. Thus, this is an important platform to spread basic knowledge to better understand the potential consequences of COVID-19.

5. Conclusions

This study shows that the coronavirus MHV-3 induces an osteoporotic phenotype in mice by triggering an inflammatory environment dependent on TNF in the bone and potentially stimulating the differentiation of osteoclasts through infection of macrophages. This is in accordance with the clinical evidence of enhanced RANKL/OPG ratio observed in severe COVID-19 patients.

Declaration of competing interest

We declare no competing financial interest in relation to this work.

Acknowledgments

This work was financially supported by grants from Coordenação de Aperfeiçoamento de Pessoal de Nível Superior–CAPES/Brazil (Projeto: CAPES - Programa: 9951 - Programa Estratégico Emergencial de Prevenção e Combate a Surtos, Endemias, Epidemias e Pandemias AUX 0641/2020 - Processo 88881.507175/2020-01). This work also received support from the National Institute of Science and Technology in Dengue and Host-Microorganism Interaction (INCT em Dengue), sponsored by the Conselho Nacional de Desenvolvimento Científico e Tecnológico (CNPq; Brazil) (Processo CNPQ: 465425/2014-3) and the Fundação de Amparo à Pesquisa do Estado de Minas Gerais (FAPEMIG; Brazil) (Processo FAPEMIG: 25036). The funding sources had no involvement in the conduction of the research and/or preparation of the article. We also acknowledge Prof. Leda Quercia Vieira for the donation of the $TNFRp55^{-/-}$ mice and Ilma Marçal de Souza and Rosemeire Oliveira for their technical assistance with experiments.

References

[1] World Health Organization W.H.O., COVID-19 Weekly Epidemiologic Update. Edition 130, 2023.
[2] M.E. Romero-Ibarguengoitia, A. González-Cantú, C. Pozzi, R. Levi, M. Mollura, R. Sarti, M.Á. Sanz-Sánchez, D. Rivera-Salinas, Y.G. Hernández-Ruíz, A. G. Armendariz-Vázquez, G.F. Del Rio-Parra, I.A. Barco-Flores, R. González-Facio,

E. Azzolini, R. Barbieri, A.R. de Azevedo Dias, M. Henriques Guimarães Júnior, A. Bastos-Borges, C. Acciardi, G. Paez-Bo, M.M. Teixeira, M. Rescigno, Analysis of immunization time, amplitude, and adverse events of seven different vaccines against SARS-CoV-2 across four different countries, Front. Immunol. 13 (2022 Jul 28), 894277, https://doi.org/10.3389/fimmu.2022.894277. PMID: 35967368; PMCID: PMC9367469.

[3] G.G. Resende, R. da Cruz Lage, S.Q. Lobê, A.F. Medeiros, Costa E. Silva AD, A. T. Nogueira Sá, Oliveira AJA, D. Sousa, H.C. Guimarães, I.C. Gomes, R.P. Souza, R. S. Aguiar, R. Tunala, F. Forestiero, J.S.S. Bueno Filho, M.M. Teixeira, Blockade of interleukin seventeen (IL-17A) with secukinumab in hospitalized COVID-19 patients - the BISHOP study, Lond, Infect. Dis. 54 (8) (2022 Aug) 591–599, https://doi.org/10.1080/23744235.2022.2066171. Epub 2022 Apr 29. PMID: 35485381.

[4] M.Z. Tay, C.M. Poh, L. Rénia, P.A. MacAry, L.F.P. Ng, The trinity of COVID-19: immunity, inflammation and intervention, Nat. Rev. Immunol. 20 (6) (2020 Jun) 363–374, https://doi.org/10.1038/s41577-020-0311-8. Epub 2020 Apr 28. PMID: 32346093; PMCID: PMC7187672.

[5] C. Huang, Y. Wang, X. Li, L. Ren, J. Zhao, Y. Hu, L. Zhang, G. Fan, J. Xu, X. Gu, Z. Cheng, T. Yu, J. Xia, Y. Wei, W. Wu, X. Xie, W. Yin, H. Li, M. Liu, Y. Xiao, H. Gao, L. Guo, J. Xie, G. Wang, R. Jiang, Z. Gao, Q. Jin, J. Wang, B. Cao, Clinical features of patients infected with 2019 novel coronavirus in Wuhan, China, Lancet 395 (10223) (2020 Feb 15) 497–506, https://doi.org/10.1016/S0140-6736(20)30183-5. Epub 2020 Jan 24. Erratum in: Lancet. 2020 Jan 30;: PMID: 31986264; PMCID: PMC7159299.

[6] G. Chen, D. Wu, W. Guo, Y. Cao, D. Huang, H. Wang, T. Wang, X. Zhang, H. Chen, H. Yu, X. Zhang, M. Zhang, S. Wu, J. Song, T. Chen, M. Han, S. Li, X. Luo, J. Zhao, Q. Ning, Clinical and immunological features of severe and moderate coronavirus disease 2019, J. Clin. Invest. 130 (5) (2020 May 1) 2620–2629, https://doi.org/10.1172/JCI137244. PMID: 32217835; PMCID: PMC7190990.

[7] N.P. Disser, A.J. De Micheli, M.M. Schonk, M.A. Konnaris, A.N. Piacentini, D. L. Edon, B.G. Toresdahl, S.A. Rodeo, E.K. Casey, C.L. Mendias, Musculoskeletal consequences of COVID-19, J. Bone Joint Surg. Am. 102 (14) (2020 Jul 15) 1197–1204, https://doi.org/10.2106/JBJS.20.00847. PMID: 32675661; PMCID: PMC7508274.

[8] L. Sapra, C. Saini, B. Garg, R. Gupta, B. Verma, P.K. Mishra, R.K. Srivastava, Long-term implications of COVID-19 on bone health: pathophysiology and therapeutics, Inflamm. Res. 71 (9) (2022 Sep) 1025–1040, https://doi.org/10.1007/s00011-022-01616-9. Epub 2022 Jul 28. PMID: 35900380; PMCID: PMC9330992.

[9] N. Chen, M. Zhou, X. Dong, J. Qu, F. Gong, Y. Han, Y. Qiu, J. Wang, Y. Liu, Y. Wei, J. Xia, T. Yu, X. Zhang, L. Zhang, Epidemiological and clinical characteristics of 99 cases of 2019 novel coronavirus pneumonia in Wuhan, China: a descriptive study, Lancet 395 (10223) (2020 Feb 15) 507–513, https://doi.org/10.1016/S0140-6736(20)30211-7. Epub 2020 Jan 30. PMID: 32007143; PMCID: PMC7135076.

[10] H.E. Davis, G.S. Assaf, L. McCorkell, H. Wei, R.J. Low, Y. Re'em, S. Redfield, J. P. Austin, A. Akrami, Characterizing long COVID in an international cohort: 7 months of symptoms and their impact, EClinicalMedicine 38 (2021 Aug), 101019, https://doi.org/10.1016/j.eclinm.2021.101019. Epub 2021 Jul 15. PMID: 34308300; PMCID: PMC8280690.

[11] J. Kottlors, N. Große Hokamp, P. Fervers, J. Bremm, F. Fichter, T. Persigehl, O. Safarov, D. Maintz, S. Tritt, N. Abdullayev, Early extrapulmonary prognostic features in chest computed tomography in COVID-19 pneumonia: bone mineral density is a relevant predictor for the clinical outcome - a multicenter feasibility study, Bone 144 (2021 Mar), 115790, https://doi.org/10.1016/j.bone.2020.115790. Epub 2020 Dec 7. PMID: 33301962; PMCID: PMC7720732.

[12] M. Tahtabasi, N. Kilicaslan, Y. Akin, E. Karaman, M. Gezer, Y.K. Icen, F. Sahiner, The prognostic value of vertebral bone density on chest CT in hospitalized COVID-19 patients, J. Clin. Densitom. 24 (4) (2021 Oct-Dec) 506–515, https://doi.org/10.1016/j.jocd.2021.07.007. Epub 2021 Jul 24. PMID: 34353732; PMCID: PMC8302819.

[13] O.D. Awosanya, C.E. Dalloul, R.J. Blosser, U.C. Dadwal, M. Carozza, K. Boschen, M. J. Klemsz, N.A. Johnston, A. Bruzzaniti, C.M. Robinson, E.F. Srour, M.A. Kacena, Osteoclast-mediated bone loss observed in a COVID-19 mouse model, Bone 154 (2022 Jan), 116227, https://doi.org/10.1016/j.bone.2021.116227. Epub 2021 Oct 2. PMID: 34607050; PMCID: PMC8486589.

[14] W. Qiao, H.E. Lau, H. Xie, V.K. Poon, C.C. Chan, H. Chu, S. Yuan, T.T. Yuen, K. K. Chik, J.O. Tsang, C.C. Chan, J.P. Cai, C. Luo, K.Y. Yuen, K.M. Cheung, J.F. Chan, K.W. Yeung, SARS-CoV-2 infection induces inflammatory bone loss in golden Syrian hamsters, Nat. Commun. 13 (1) (2022 May 9) 2539, https://doi.org/10.1038/s41467-022-30195-w. Erratum. In: Nat Commun. 2022 May 31;13(1): 3139. PMID: 35534483; PMCID: PMC9085785.

[15] G. Tatangelo, J. Watts, K. Lim, C. Connaughton, J. Abimanyi-Ochom, F. Borgström, G.C. Nicholson, C. Shore-Lorenti, A.L. Stuart, S. Iuliano-Burns, E. Seeman, R. Prince, L. March, M. Cross, T. Winzenberg, L.L. Laslett, G. Duque, P.R. Ebeling, K.M. Sanders, The cost of osteoporosis, osteopenia, and associated fractures in Australia in 2017, J. Bone Miner. Res. 34 (4) (2019 Apr) 616–625, https://doi.org/10.1002/jbmr.3640. Epub 2019 Jan 7 PMID: 30615801.

[16] J. Patel, Economic implications of osteoporotic fractures in postmenopausal women, Am. J. Manag. Care 26 (15 Suppl) (2020 Nov) S311–S318, https://doi.org/10.37765/ajmc.2020.88549. PMID: 33263967.

[17] C. Muñoz-Fontela, W.E. Dowling, S.G.P. Funnell, P.S. Gsell, A.X. Riveros-Balta, R. A. Albrecht, H. Andersen, R.S. Baric, M.W. Carroll, M. Cavaleri, C. Qin, I. Crozier, K. Dallmeier, L. de Waal, E. de Wit, L. Delang, E. Dohm, W.P. Duprex, D. Falzarano, C.L. Finch, M.B. Frieman, B.S. Graham, L.E. Gralinski, K. Guilfoyle, B.L. Haagmans, G.A. Hamilton, A.L. Hartman, S. Herfst, S.J.F. Kaptein, W.B. Klimstra, I. Knezevic, P.R. Krause, J.H. Kuhn, R. Le Grand, M.G. Lewis, W.C. Liu, P. Maisonnasse, McElroy AK, V. Munster, N. Oreshkova, A.L. Rasmussen, J. Rocha-Pereira, B. Rockx, E. Rodríguez, T.F. Rogers, F.J. Salguero, M. Schotsaert, K.J. Stittelaar, H. J. Thibaut, C.T. Tseng, J. Vergara-Alert, M. Beer, T. Brasel, Chan JFW, A. García-Sastre, J. Neyts, S. Perlman, D.S. Reed, J.A. Richt, C.J. Roy, J. Segalés, S.S. Vasan, A.M. Henao-Restrepo, D.H. Barouch, Animal models for COVID-19, Nature 586 (7830) (2020 Oct) 509–515, https://doi.org/10.1038/s41586-020-2787-6. Epub 2020 Sep 23. PMID: 32967005; PMCID: PMC8136862.

[18] A.C.D.S.P. Andrade, G.H. Campolina-Silva, C.M. Queiroz-Junior, L.C. de Oliveira, L.S.B. Lacerda, J.C.P. Gaggino, F.R.O. de Souza, I. de Meira Chaves, I.B. Passos, D. C. Teixeira, P.G. Bittencourt-Silva, Valadão PAC, L. Rossi-Oliveira, M.M. Antunes, Figueiredo AFA, N.T. Wnuk, J.R. Temerozo, A.C. Ferreira, A. Cramer, C.A. Oliveira, R. Durães-Carvalho, C. Weis Arns, P.P.G. Guimarães, G.M.J. Costa, G.B. de Menezes, C. Guatimosim, G.S.F. da Silva, T.M.L. Souza, B.R. Barrioni, M.M. Pereira, L.P. de Sousa, M.M. Teixeira, V.V. Costa, A biosafety level 2 mouse model for studying betacoronavirus-induced acute lung damage and systemic manifestations, J. Virol. 95 (22) (2021 Oct 27), e0127621, https://doi.org/10.1128/JVI.01276-21. Epub 2021 Sep 8. PMID: 34495692; PMCID: PMC8549505.

[19] R.W. Körner, M. Majjouti, M.A.A. Alcazar, E. Mahabir, Of mice and men: the coronavirus MHV and mouse models as a translational approach to understand SARS-CoV-2, Viruses 12 (8) (2020 Aug 12) 880, https://doi.org/10.3390/v12080880. PMID: 32806708; PMCID: PMC7471983.

[20] P.P. Liu, A. Blet, D. Smyth, H. Li, The science underlying COVID-19: implications for the cardiovascular system, Circulation 142 (1) (2020 Jul 7) 68–78, https://doi.org/10.1161/CIRCULATIONAHA.120.047549. Epub 2020 Apr 15 PMID: 32293910.

[21] M.A. Khalili, K. Leisegang, A. Majzoub, R. Finelli, M.K. Panner Selvam, R. Henkel, M. Mojgan, A. Agarwal, Male fertility and the COVID-19 pandemic: systematic review of the literature, World J. Mens.Health 38 (4) (2020 Oct) 506–520, https://doi.org/10.5534/wjmh.200134. Epub 2020 Aug 14. PMID: 32814369; PMCID: PMC7502312.

[22] L. Mancini, L.M. Americo, T. Pizzolante, R. Donati, E. Marchetti, Impact of COVID-19 on periodontitis and peri-implantitis: a narrative review, Front. Oral Health 3 (2022 Feb 10), 822824, https://doi.org/10.3389/froh.2022.822824. PMID: 35224542; PMCID: PMC8866640.

[23] P.S. Timiras, Disuse and aging: same problem, different outcomes, J. Gravit. Physiol. 1 (1) (1994 May) P5–P7. PMID: 11538760.

[24] E.M. Lau, F.W. Chan, D.S. Hui, A.K. Wu, P.C. Leung, Reduced bone mineral density in male severe acute respiratory syndrome (SARS) patients in Hong Kong, Bone 37 (3) (2005 Sep) 420–424, https://doi.org/10.1016/j.bone.2005.04.018. PMID: 15993669; PMCID: PMC7103402.

[25] S. Ran, S. Zhang, H. Chen, M. Zhao, B. Liu, Total body bone mineral density and severe COVID-19: a Mendelian randomization analysis in five age strata, Bone 155 (2022 Feb), 116281, https://doi.org/10.1016/j.bone.2021.116281. Epub 2021 Dec 1. PMID: 34863930; PMCID: PMC8634701.

[26] D. Pamart, M. Otekpo, M. Asfar, G. Duval, J. Gautier, C. Annweiler, Hypercalcemia as a biomarker of poor prognosis in frail elderly patients with COVID-19, J. Nutr. Health Aging 25 (10) (2021) 1140–1144, https://doi.org/10.1007/s12603-021-1690-7. PMID: 34866140; PMCID: PMC8527973.

[27] N. Takegahara, H. Kim, Y. Choi, RANKL biology, Bone 159 (2022 Jun), 116353, https://doi.org/10.1016/j.bone.2022.116353. Epub 2022 Feb 16. PMID: 35181574; PMCID: PMC9035122.

[28] S.W. Barthold, A.L. Smith, Mouse hepatitis virus strain–related patterns of tissue tropism in suckling mice, Arch. Virol. 81 (1–2) (1984) 103–112, https://doi.org/10.1007/BF01309300. PMID: 6331343; PMCID: PMC7086666.

[29] W. Feng, J. Guo, M. Li, RANKL-independent modulation of osteoclastogenesis, J. Oral Biosci. 61 (1) (2019 Mar) 16–21, https://doi.org/10.1016/j.job.2019.01.001. Epub 2019 Jan 11. Erratum in: J Oral Biosci. 2020 Sep;62(3): 298. PMID: 30929797.

[30] C.M. Queiroz-Junior, A.C.P.M. Santos, I. Galvão, G.R. Souto, R.A. Mesquita, M. A. Sá, A.J. Ferreira, The angiotensin converting enzyme 2/angiotensin-(1–7)/Mas receptor axis as a key player in alveolar bone remodeling, Bone 128 (2019 Nov), 115041, https://doi.org/10.1016/j.bone.2019.115041. Epub 2019 Aug 20 PMID: 31442676.

[31] S. Obitsu, N. Ahmed, H. Nishitsuji, A. Hasegawa, K. Nakahama, I. Morita, K. Nishigaki, T. Hayashi, T. Masuda, M. Kannagi, Potential enhancement of osteoclastogenesis by severe acute respiratory syndrome coronavirus 3a/X1 protein, Arch. Virol. 154 (9) (2009) 1457–1464, https://doi.org/10.1007/s00705-009-0472-z. Epub 2009 Aug 14. PMID: 19685004; PMCID: PMC7086770.

[32] C. Junqueira, Â. Crespo, S. Ranjbar, L.B. de Lacerda, M. Lewandrowski, J. Ingber, B. Parry, S. Ravid, S. Clark, M.R. Schrimpf, F. Ho, C. Beakes, J. Margolin, N. Russell, K. Kays, J. Boucau, U. Das Adhikari, S.M. Vora, V. Leger, L. Gehrke, L. A. Henderson, E. Janssen, D. Kwon, C. Sander, J. Abraham, M.B. Goldberg, H. Wu, G. Mehta, S. Bell, A.E. Goldfeld, M.R. Filbin, J. Lieberman, FcγR-mediated SARS-CoV-2 infection of monocytes activates inflammation, Nature 606 (7914) (2022 Jun) 576–584, https://doi.org/10.1038/s41586-022-04702-4. Epub 2022 Apr 6 PMID: 35385861.

[33] M.M. Rajah, A. Bernier, J. Buchrieser, O. Schwartz, The mechanism and consequences of SARS-CoV-2 spike-mediated fusion and syncytia formation, J. Mol. Biol. 434 (6) (2022 Mar 30), 167280, https://doi.org/10.1016/j.jmb.2021.167280. Epub 2020 Jan 24. Erratum in: Lancet. 2020 Jan 30;: PMID: 31986264; PMCID: PMC7159299.

[34] R. Chen, Z. Lan, J. Ye, L. Pang, Y. Liu, W. Wu, X. Qin, Y. Guo, P. Zhang, Cytokine storm: the primary determinant for the pathophysiological evolution of COVID-19

deterioration, Front. Immunol. 28 (12) (2021 Apr), 589095, https://doi.org/10.3389/fimmu.2021.589095. PMID: 33995341; PMCID: PMC8115911.

[35] H. Hachem, A. Godara, C. Schroeder, D. Fein, H. Mann, C. Lawlor, J. Marshall, A. Klein, D. Poutsiaka, J.L. Breeze, R. Joshi, P. Mathew, Rapid and sustained decline in CXCL-10 (IP-10) annotates clinical outcomes following TNFα-antagonist therapy in hospitalized patients with severe and critical COVID-19 respiratory failure, J. Clin. Transl. Sci. 5 (1) (2021 Jun 25), e146, https://doi.org/10.1017/cts.2021.805. PMID: 34457357; PMCID: PMC8376916.

[36] M. Feldmann, R.N. Maini, J.N. Woody, S.T. Holgate, G. Winter, M. Rowland, D. Richards, T. Hussell, Trials of anti-tumour necrosis factor therapy for COVID-19 are urgently needed, Lancet 395 (10234) (2020 May 2) 1407–1409, https://doi.org/10.1016/S0140-6736(20)30858-8. Epub 2020 Apr 9. PMID: 32278362; PMCID: PMC7158940.